NASA-TM-100183 19880016993

NASA Technical Memorandum 100183

Computer Simulation of Multiple Pilots Flying a Modern High Performance Helicopter

Mark E. Zipf, William G. Vogt, Marlin H. Mickle,
Ronald G. Hoelzeman, and Fei Kai
University of Pittsburgh
Pittsburgh, Pennsylvania

and

James R. Mihaloew
Lewis Research Center
Cleveland, Ohio

July 1988

NASA

COMPUTER SIMULATION OF MULTIPLE PILOTS FLYING A MODERN HIGH-PERFORMANCE HELICOPTER

Mark E. Zipf,* William G. Vogt,* Marlin H. Mickle,*
Ronald G. Hoelzeman,* and Fei Kai*
Department of Electrical Engineering
University of Pittsburgh
Pittsburgh, Pennsylvania

and

James R. Mihaloew
National Aeronautics and Space Administration
Lewis Research Center
Cleveland, Ohio

SUMMARY

A computer simulation of a human response pilot mechanism within the flight control loop of a high-performance modern helicopter is presented. A human response mechanism, implemented by a low-order, linear transfer function, is used in a decoupled single-variable configuration that exploits the dominant vehicle characteristics by associating cockpit controls and instrumentation with specific vehicle dynamics. Low-order helicopter models obtained from evaluations of the time and frequency domain responses of a nonlinear simulation model, provided by NASA Lewis Research Center, are presented and considered in the discussion of the pilot development. Pilot responses and reactions to test maneuvers are presented and discussed. Higher level implementation, using the pilot mechanisms, are discussed and considered for their use in a comprehensive control structure.

INTRODUCTION

When considering human-piloted flight-control environments, the pilot must contend with a large number of tasks that are associated with the overall operation of the aircraft. The most basic objective is to achieve stabilized control over the vehicle's attitudes, rates, and orientations. This is the central component of any operation that requires maneuvering the vehicle and should therefore be considered the most fundamental control function that a pilot executes.

A command-based cascaded control loop structure associated with pilot-based flight control is shown in figure 1. This structure was used to investigate a model of human pilot behavior within the flight control loops of a modern high-performance helicopter. This control configuration is based on the assumption that the pilot obtains feedback primarily through visual inspection of the cockpit instrumentation and external visual cues. Thus, the pilot's dependence on visually based feedback presents a significant problem, due to the limitations of the human visual system's information processing capabilities. These limitations restrict the pilot's ability to simultaneously monitor

---

*Work funded by NASA Grant NAG 3-729.

and control the appropriate states of the aircraft. For the purpose of simulation, the pilot observes and considers only one control variable at a time. Thus, the flight control loop implementation is organized in such a way that manipulating one specific cockpit control mechanism is based on the instrument or external visual cue as shown in figure 2.

The single-variable control of this configuration presents a significant task because of the helicopter's strongly coupled behavior. The lack of control over the secondary response characteristics can promote widespread variations in vehicle orientation. To create a suitable control configuration, the pilot is forced to rely only on an understanding of the dominant response characteristics of the helicopter. The dominant responses are considered to be the most pronounced variation of a vehicle attitude or rate, due to a deflection of a cockpit control mechanism. The secondary responses are the remaining vehicle reactions, which may be coupled to the primary response.

The remainder of this report presents and discusses the development of a set of singular human response pilot mechanisms for use in the flight control loops of a high-performance helicopter. The main approach is to determine the necessary single-variable control features of the individual pilot mechanisms. These mechanisms are considered to be ideal, in the sense that the intrinsic random behavior of the human is neglected so as to investigate only the fundamental control-based responses. Implementing the random behavior processes is discussed for use in actual pilot operations. The set of singular mechanisms provides the foundation for higher level pilot implementations. Pilot evaluations have been conducted by direct insertion into the previously indicated nonlinear simulation model (ref. 1) provided by NASA. The pilot responses and reactions to test operations are presented and discussed.

NOMENCLATURE

ALT(S)	Laplacian of altitude position, ft
ALTDT(S)	Laplacian of vertical rate, ft/sec
a	time constant
a_{ALT}	pole time constant of altitude models, sec^{-1}
a_{PSL}	compensative zero time constant for low-speed heading control pilot, sec^{-1}
b_{PSL}	compensative pole time constant for low-speed heading control pilot, sec^{-1}
CG	center of gravity of vehicle
COLL(S)	Laplacian of main rotor collective stick deflection, in.
D	time constant of total lag of human response model, sec

F_0	longitudinal main rotor forward thrust component prior to maneuver
F_1	longitudinal main rotor forward thrust component after maneuver
$G_{ALT}(S)$	transfer function of main rotor collective stick to altitude, ft/in.
$G_{ALTDT}(S)$	transfer function of main rotor collective stick to vertical rate, ft/(in.-sec)
$G_{PHI}(S)_{20,40}$	low-speed transfer function of lateral cyclic stick to roll angle, deg/in.
$G_{PHI}(S)_{60,80,100}$	high-speed transfer function of lateral cyclic stick to roll angle, deg/in.
$G_{PLT}(S)$	single-variable linear transfer function of human response mechanism
$G_{PLT}^{ALT}(S)$	transfer function of human response altitude control pilot, in./ft
$G_{PLT}^{ALTDT}(S)$	transfer function of human response vertical rate control pilot, in.-sec/ft
$G_{PLT}^{PHI}(S)_{20,40}$	transfer function of human response roll control pilot for low speeds, in./deg
$G_{PLT}^{PHI}(S)_{60,80,100}$	transfer function of human response roll control pilot for high speeds, in./deg
$G_{PLT}^{PSI}(S)_{20,40}$	transfer function of human response heading control pilot for low speeds, in./deg
$G_{PLT}^{PSI}(S)_{60,80,100}$	transfer function of human response headng control pilot for high speeds, in./deg
$G_{PLT}^{PHYS}(S)$	transfer function of physical representation in human response model
$G_{PLT}^{THETA}(S)$	transfer function of human response pitch control pilot, in./deg
$G_{PSI}(S)_{20,40}$	low-speed transfer function of tail rotor collective pedals to yaw angle, deg/in.
$G_{PSI}(S)_{60,80,100}$	high-speed transfer function of tail rotor collective pedals to yaw angle, deg/in.
$G_{THETDT}(S)$	transfer function of longitudinal cyclic stick to pitch rate, rad/(in.-sec)

$G_{THETA}(S)$	transfer function of longitudinal cyclic stick to pitch angle, deg/in.
g	gravitational acceleration, ft/sec^2
Hp(S)	single-variable transfer function of primary response
$H_S(S)$	multivariable transfer function of secondary responses
K	forward path gain of human response transfer function compensation block (units depend on application)
K_{ALT}	gain of vehicle altitude model, $(sec^2)^{-1}$
K_{ALTDT}	gain of vehicle vertical rate model, sec-1
K_{PA}	gain of altitude control pilot, $(sec^2)^{-1}$
K_{PAD}	gain of vertical rate control pilot, sec^{-1}
K_{PSH}	gain of high-speed heading control pilot, $in./sec^2$
K_{PSL}	gain of low-speed heading control pilot, $in./sec^2$
K_{PT}	gain of pitch control pilot, $in./sec^2$
K_{SH}	gain of high-speed heading models, $(in.-sec^3)^{-1}$
K_{SL}	gain of low-speed heading models, $(in.-sec^3)^{-1}$
K_T	gain of vehicle pitch angle model, $(in.-sec^2)^{-1}$
K_{TD}	gain of vehicle pitch rate model, $(in.-sec^3)^{-1}$
L_0	longitudinal main rotor lift component prior to maneuver
L_1	longitudinal main rotor lift component after maneuver
L_0'	lateral component of main rotor lift prior to maneuver
L_1'	lateral component of main rotor lift after maneuver
LAT(S)	Laplacian of lateral cyclic stick, in.
LONG(S)	Laplacian of longitudinal cyclic stick deflection, in.
m	vehicle mass, slugs
N	order of human response lag approximation
$P_{ED}(S)$	Laplacian of tail rotor collective pedal deflection, in.
$P_{HI}(S)$	Laplacian of roll angle, deg

$P_{SI}(S)$	Laplacian of yaw angle, deg
P_b	perturbation roll rate along body axis, rad/sec
QB	pitch rate, rad/sec
q_b	perturbation pitch rate along body axis, rad/sec
r_b	perturbation yaw rate along body axis, rad/sec
S	Laplacian variable
S_0	lateral component of main rotor thrust vector prior to maneuver
S_1	lateral component of main rotor thrust vector after maneuver
T	time constant of human lag approximation, sec
T_a	time constant of the action lag, sec
T_c	time constant of information processing lag, sec
T_k	time constant of transmission zero of human response compensation block, sec
T_m	time constant of pole of human response compensation block, sec
T_n	time constant of pole of muscular system model, sec
T_v	time constant of visual system lag, sec
T_{R0}	tail rotor thrust prior to maneuver
T_{R1}	tail rotor thrust after maneuver
T_0	longitudinal main rotor thrust component prior to maneuver
T_1	longitudinal main rotor thrust component after maneuver
T_0'	main rotor thrust vector in lateral plane prior to maneuver
T_1'	main rotor thrust vector in lateral plane after maneuver
THETDT(S)	Laplacian of pitch rate, rad/sec
THETA(S)	Laplacian of pitch angle, deg
u_b	velocity perturbation along X body, ft/sec
V	vehicle velocity
v_b	velocity perturbation along Y body, ft/sec

w_b	velocity perturbation along Z body, ft/sec
w_P	natural frequency of roll angle models, rad/sec
w_{S1}	natural frequency of dominant poles of low-speed heading models, rad/sec
w_{S2}	natural frequency of resonant zeroes of low-speed heading models, rad/sec
w_{S3}	natural frequency of resonant poles of low-speed heading models, rad/sec
w_T	natural frequency of pitch models, rad/sec
x_b	X-body component
y_b	Y-body component
z_b	Z-body component
α_0	longitudinal main rotor angle of attack prior to maneuver
α_1	longitudinal main rotor angle of attack after maneuver
δ_P	damping ratio of roll angle models
δ_{S1}	damping ratio of dominant poles of low-speed heading models
δ_{S2}	damping ratio of resonant zeroes of low-speed heading models
δ_{S3}	damping ratio of resonant poles of low-speed heading models
δ_T	damping ratio of pitch models
ψ_0	vehicle heading prior to maneuver, deg
ψ_1	vehicle heading after maneuver, deg

HUMAN RESPONSE MODEL

The linear transfer function model of human responses that is used in this discussion is given in reference 2 and shown in figure 3. The resulting transfer function is given by

$$G_{PLT}(S) = \frac{K(T_k S + 1)e^{-DS}}{(T_m S + 1)(T_n S + 1)} \qquad (1)$$

This model assumes a cascaded configuration and uses assessments of visually based information to produce compensative control mechanism deflections that

achieve the desired response characteristics. Human mannerisms are represented by associating physical and judgmental response attributes to the specific parameters of the transfer function. Human traits tend to limit the operational performance of the pilot.

The physical attributes are regarded as the physiological abilities and limitation of the mechanisms that the human relies on to carry out the control and compensation reactions. The judgmental or equalization attributes furnish the compensating parameters that the pilot uses within the control loop. These parameters specify the manner in which the human reacts when confronted with a certain control/stabilization situation.

As previously discussed, the human response models that are used in the following discussion are considered to be ideal or zero remnant/nonrandom. Implementing a somewhat more realistic human response model is accomplished by augmenting a remnant (ref. 2) control action. This provides an overall degree of uncertainty that accounts for a wide variety of random behaviors that can be attributed to humans.

SIMULATION ENVIRONMENT AND MODELS

The principal tool used to examine the helicopter and to evaluate the pilot models was a real time simulation program (ref. 1) provided by NASA Lewis. This program, developed by NASA Ames, implements a nonlinear mathematical model developed by Sikorsky. The model is a total force, large angle, nonlinear representation, in six rigid body degrees of freedom. Rotor blade flapping, lagging, and hub rotational degrees of freedom are also implemented. In addition, the simulation environment implements the primary mechanical and automated stability/flight control systems (stability augmentation system (SAS), flight path stabilizer (FPS), pitch bias actuator (PBA), and tail stabilator control (TSC)).

The low-order linear flight-control structure that is presented requires a linear representation of the helicopter's flight dynamics. The overall complexity of the nonlinear model makes any form of direct linearization very difficult. A linear, point mass, small perturbation state space model for the high-performance helicopter (ref. 3) was used initially. This model is linearized about trimmed flight conditions and considers only the vehicle dynamics. Augmenting this model with the actuation and automated systems created a model whose complexities rivaled those of the nonlinear model. The high order of this overall linear model tended to overwhelm the design and evaluation of the low-order pilot model. In addition, the state model showed some inadequacies due to its seemingly nonrobust behavior. This model did, however, reveal certain characteristics that suggested the decoupling scheme that was adopted and is discussed subsequently.

The low-order models developed and used in the design of the pilot models in this research were obtained by an analysis of the time and frequency responses of the computer-simulated helicopter's flight dynamics. These models indicate the most fundamental aspects of the helicopter's behavior and provide insight into the basic features of the compensation needed to achieve an adequate control.

INVESTIGATION OF THE DOMINANT FLIGHT CHARACTERISTICS

This section presents the development of a set of low-order transfer function models that are based on an investigation of the fundamental behavior of the helicopter simulation. The low-order models describe the primary, low-frequency vehicle reactions that are induced by deflections of specific cockpit control mechanisms. These models are intended to identify the strongest operational modes of the specific control mechanisms.

The vehicle reactions that are generated by operating a cockpit control mechanism can be characterized by two components: a primary/dominant response and the set of secondary responses (fig. 4).

The control mechanisms are the lateral and longitudinal cyclic stick, main rotor collective stick, and the tail rotor collective pedals. The vehicle responses are the Euler angles (yaw, pitch, roll), angular rates, altitude components, velocity components, etc.

The dominant vehicle reactions were identified by the direct evaluation of the nonlinear model computer simulation's time and frequency responses due to impulse and step deflections of the cockpit control mechanisms. The frequency responses were obtained by fast Fourier transforms of the time responses. It was necessary to sufficiently excite this frequency region to achieve an adequate ultra-low-frequency response. Two methods were used: (1) administering very long duration tests (>100 sec), and (2) injecting ultra-low-frequency sinusoids. Both techniques tended to promote ultra-low-frequency distortions which were caused by the interactions and couplings of the secondary variables. The time responses provided insight into the sources of the distortions and irregularities that were attributed to these occurrences.

The response tests were conducted while in trimmed forward flight at velocities of 20, 40, 60, 80, and 100 knots (kn). The initial tests were carried out with all automatic onboard control systems disengaged. The findings suggested instabilities that were characterized by low-frequency divergence. The pitch bias actuator, tail stabilator control, and stability augmentation systems (digital and analog) were engaged to enhance the flight characteristics of the helicopter. This provided a substantial improvement in the vehicle reactions.

To structure the investigation, a degree of initial decoupling was achieved by separating the control and response characteristics of the helicopter into two sets: the longitudinal control set and the lateral-directional control set. These sets consider the effects of the control mechanisms on the orientation of the helicopter within specific orthogonal planes. The orientation of the helicopter within these planes is shown in figure 5. Note that although these sets are coupled their control procedures can be separated. The vehicle and aerodynamic variables that are considered in this discussion are defined in the appendix.

For the context of this and the remaining discussions, the dynamics and overall accuracies and distortions of the cockpit instrumentation are not considered.

LONGITUDINAL CONTROL SET MODELS

The longitudinal control set specified the control mechanisms and their associated reactions whose dominant effects primarily exist in the X,Z-body plane. The longitudinal cyclic stick controls the direction of the main rotor thrust vector, in the X,Z-body plane, by controlling the angle of attack of the main rotor blade disk (fig. 6). This and the remaining pictorial descriptions are exaggerated to clarify relations between variables. Variations of the thrust vector within this plane primarily affect the forward velocity and the body pitch angle. This control mechanism also has an effect on the helicopter's altitude components. Disturbances in the other control planes can be expected because of the modifications of the main rotor's thrust vector. The main rotor collective stick controls the magnitude of the main rotor thrust vector by controlling the angle of attack of each blade of the main rotor by the same amount. The primary effect is on the lift vector; thus, the altitude and vertical rate dominate in this control mechanism (fig. 7). This mechanism effectively adjusts how much the main rotor "digs" into the atmosphere and thus can create severe main rotor torque reaction disturbances in the other control planes.

Pitch Angle Model

This model considers the primary characteristics of the pitch angle response due to operating the longitudinal cyclic stick. The time-based, impulse responses of the pitch rate QB at 60 and 100 kn can be seen in figures 8 and 9. These show a damped sinusoidal behavior whose damping ratio decreases with increasing forward velocity. In addition, the 100-kn response shows the high-frequency vibrations of the main rotor blade flapping. The frequency response of the pitch rate at 60 kn is shown in figure 10. The frequency response characteristics lend themselves to an S-plane configuration similar to that shown in figure 11(a). This configuration does not account for the ultra-low-frequency behavior shown in figure 10. The frequency response of the pitch angle (fig. 12) shows the expected integrating characteristics. In addition, figure 12 shows what appears to be a low-frequency notch feature near $w = 0.03$ rad/sec. The notch appears to be part of a peak-notch pair that is not completely visible because of the low-frequency test limitations. Figure 11(b) shows the type of response characteristics that are believed to exist in the pitch reaction. The S-plane configuration for this type of response is shown in figure 11(c). The transfer function associated with the simplified S-plane configuration is given by

$$G_{THETDT}(S) = \frac{THETDT(S)}{LONG(S)} \simeq \frac{K_{TD}}{S^2 + 2\delta_T w_T S + w_T^2} \qquad (2)$$

Evaluations of the pitch rate's damping envelopes and frequency responses reveal the following:

V, kn	w_T, rad/sec	δ_T	K_{TD}, $(in.-sec^3)^{-1}$	K_T, $(in.-sec^2)^{-1}$
20	4.7	0.28	0.041	2.32
40	4.9	.19	.045	2.59
60	5.1	.14	.051	2.91
80	5.4	.10	.049	2.83
100	5.7	.07	.048	2.77

The low-order approximation for the longitudinal cyclic's effect on the pitch angle can be summarized as

$$G_{THETA}(S) = \frac{THETA(S)}{LONG(S)} = \frac{K_T}{S\left(S^2 + 2\delta_T w_T S + w_T^2\right)} \tag{3}$$

This model does not consider the resonant behavior that can be induced by operating the longitudinal cyclic stick.

Vertical Rate Model

This model considers the vertical rate responses due to operating the collective control mechanism. Evaluations of the high-performance helicopter's reactions to the test inputs applied to the main rotor collective stick suggest the following transfer function description:

$$G_{ALTDT}(S) = \frac{ALTDT(S)}{COLL(S)} \simeq \frac{K_{ALTDT}}{S + a_{ALT}} \tag{4}$$

The corresponding parameters are as follows:

V, kn	K_{ALTDT}, $(sec^2)^{-1}$	a_{ALT}, sec^{-1}
20	6.6	0.30
40	7.0	.45
60	7.0	.50
80	7.3	.50
100	7.5	.50

This model does not consider the resonant behavior that can be induced by operating this control mechanism.

Altitude Model

This model is the pure integration of the vertical rate model. The altitude response model is given by

$$G_{ALT}(S) = \frac{ALT(S)}{COLL(S)} \simeq \frac{K_{ALT}}{S(S + a_{ALT})} \tag{5}$$

LATERAL-DIRECTIONAL CONTROL SET MODELS

The lateral-directional control set specifies the reactions and their associated control mechanisms whose dominant effects are in the Y,Z-body plane (lateral) and the X,Y-body plane (directional). The fundamental maneuvering characteristics of this set tend to orient the vehicle in such a way that the aerodynamic profiles induce drag-related responses. The lateral cyclic stick controls the lateral (Y,Z-plane) direction of the main rotor's thrust vector (fig. 13). Variations in the lateral plane of the main rotor thrust vector primarily affect the lateral velocity and the body roll angle. The cosine related reduction in the vertical lift component affects the altitude components. The tail rotor collective pedals control the magnitude and direction of the tail rotor's thrust vector by altering the angle of attack of each blade of the tail rotor. Variations in the tail rotor's thrust induce torqued rotations about the Z-body axis which result in yawing motions (fig. 14). The pedal's effect on the yaw/heading angle promotes its use in directional regulation. In addition, the pedals are the primary candidate to counteract the torque-induced reaction disturbances of the main rotor.

Roll Angle Model

This model considers the fundamental aspects of the body roll angle due to operating the lateral cyclic. An analysis of the test results indicated two slightly different response characteristics, one for low speeds (20 to 40 kn) and one for high speeds (60 to 100 kn). This behavior has been attributed to the mode switching of the yaw SAS near 60 kn. The low-speed model is given by the transfer function

$$G_{PHI}(S)_{20,40} = \frac{PHI(S)}{LAT(S)} \simeq \frac{820}{S\left(S^2 + 2\delta_P w_P S + w_P^2\right)^2} \tag{6}$$

and the high-speed model is given by

$$G_{PHI}(S)_{60,80,100} = \frac{PHI(S)}{LAT(S)} \simeq \frac{210(S + 3)}{S\left(S^2 + 2\delta_P w_P S + w_P^2\right)^2} \tag{7}$$

These models do not show the resonant behavior that can be seen in the responses. Figure 15 shows the frequency response of the roll rate at 80 kn. Substantial peak-notch-type characteristics can be seen near 2 and 22 rad/sec. The high-frequency resonance is attributed to the main rotor blade flap. The

lower frequency resonance is in a troublesome frequency region because the pilot attempts to achieve a closed loop within this frequency bandwidth.

Heading/Directional Yaw Angle Model

This model considers the dominant effects of the tail rotor collective pedals on the helicopter's heading. The test results show a strong integrating tendency at all forward velocities. The higher speeds show signs of aerodynamic influences which tend to cause weather vane effects. These effects are due to aerodynamically induced torques that tend to realign the fuselage with the forward velocity vector. This torque makes it difficult to maintain fixed yaw orientations that correspond to large sideslip angles when operating at higher speeds.

An analysis of the lower velocity frequency responses (fig. 16) shows a moderate peak-notch characteristic near 2 rad/sec. The properties of the yaw rate suggest a low-speed S-plane representation for the yaw angle (fig. 17). Thus, the following relation was developed for the yaw angle at low speeds:

$$G_{PSI}(S)_{20,40} = \frac{PSI(S)}{PED(S)} \simeq \frac{K_{SL}}{S\left(S^2 + 2\delta_{S1}w_{S1}S + w_{S1}^2\right)}\left(\frac{S^2 + 2\delta_{S2}w_{S2}S + w_{S2}^2}{S^2 + 2\delta_{S3}w_{S3}S + w_{S3}^2}\right) \tag{8}$$

An examination of the frequency and time responses suggests the following approximate relations:

V, kn	K_{SL}, $(in.-sec^3)^{-1}$	w_{S1}, rad/sec	δ_{S1}, dimensionless	w_{S2}, rad/sec	δ_{S2}, dimensionless	w_{S3}, rad/sec	δ_{S3}, dimensionless
20	87	3.5	0.3	2.5	0.1	2.2	0.15
40	32	3.5	.4	1.8	.1	2.0	.15

The higher speed operations did not suffer from the problems that plagued the lower speed models and therefore relied only on the representation

$$G_{PSI}(S)_{60,80,100} = \frac{PSI(S)}{PED(S)} \simeq \frac{K_{SH}}{S} \tag{9}$$

The gain profile is

V, kn	K_{SH}, $(in.-sec)^{-1}$
60	3.5
80	3.1
100	2.4

PILOT IMPLEMENTATIONS

The single-variable control configuration that is used for the analysis and operation of the pilot mechanism is shown in figure 18. This type of configuration allows the control of only the primary variable. The reactions that occur in the secondary variables are considered to be disturbances. The structure of the human response mechanism limits the form of compensation to a lead-lag/lag-lead type configuration. This arrangement provided an acceptable pilot control framework that was directly applied to the low-order helicopter models via root locus techniques.

An important factor that could not be overlooked was the lag associated with the human visual and information processing system. In the continuous time domain, this lag corresponds to an infinite number of poles at $S = -\infty$ on the real axis. These poles introduce an infinite number of asymptotes that are parallel to the real axis and result in significant destabilizing distortions of the asymptotic behavior of the root locus as shown in figure 19. The main problem in dealing with the delayed root locus is that most of the non-delayed assumptions are no longer valid. For the purpose of the design and analysis, the pure delay was approximated by

$$e^{-TS} \simeq \frac{1}{\left(1 + \frac{T}{N}S\right)^2} \tag{10}$$

To remain within computational limits, 20 poles were placed at -100 on the real axis. The primary asymptote of this pole group had a 9° angle of incidence and an imaginary axis intercept near 15.84 (15.71 for the ideal pure delay), as illustrated in figure 20. This approximation allowed the complete use of all nondelayed assumptions.

To adhere to the physical limitations of human reactions, the time constant associated with muscular response was set at 0.1 sec. The delay associated with the visual/neurological lag was set at 0.2 sec. The resulting common physical pilot configuration was

$$G_{PLY}^{PHYS}(S) = \frac{e^{-0.25}}{(S + 10)} \tag{11}$$

The human response model, which has been discussed, is a continuous time representation. Within the simulation environment, a zero-order-hold discrete time representation was used. The pilot development strategy consisted of a continuous time domain design with root locus techniques and then transformation into the discrete time domain for direct insertion into the simulation environment.

The remainder of this section presents the designs and implementations of the individual pilots. Since many of the helicopter models have high-frequency complex poles that are precariously close to the right half plane, care must be taken to ensure that these poles do not migrate into the right half plane. In addition, the resonant behavior, described previously, must be considered. Gain limitation and reduced closed-loop bandwidths may be unavoidable because of these problems.

Altitude Control Pilot

This pilot provides a position control of the vehicle altitude by visual assessment of the altimeter and deflection of the main rotor collective. The human response limitations imposed on the compensating zero ($a \geq 0.8$) dictate a type 1 implementation. The type 1 structure provides a zero error track of step commands and disturbances. This may induce offset operations when ramp-type disturbances are introduced into the altitude control. Initially, the dominant closed-loop poles were positioned near $w = 3$ rad/sec, $\delta = 0.8$. When inserted into the nonlinear simulation program, the pilot tended to excite resonant behavior in the X-Y (yaw) plane at all forward velocities. To reduce the resonance problems, the loop was closed near $w = 1.45$ rad/sec, $\delta = 0.75$. The resulting single-variable transfer function of the pilot mechanism is given by

$$G_{PLT}^{ALT}(S) = \frac{K_{PA}(S + 0.8)e^{-0.2S}}{(S + 5.5)(S + 10)} \tag{12}$$

The gain profile is

V, kn	K_{PA}
20	5.77
40	5.68
60	4.97
80	5.07
100	5.19

Vertical Rate Pilot

This pilot provides a rate control of the vehicle altitude by monitoring the vertical rate indicator and operating the main rotor collective. The pilot furnishes the integration component and therefore provide a type 1 configuration. Again, this type of system is not capable of zero error tracking ramps or higher order disturbances. Closing the loop near $w = 3.0$ rad/sec caused resonant excitation. The dominant closed-loop poles were placed near $w = 1.3$ rad/sec and $\delta = 0.65$. The pilot mechanism's single-variable transfer function is given by

$$G_{PLT}^{ALTDT}(S) = \frac{K_{PAD}(S + 0.8)e^{-0.25}}{S(S + 10)} \tag{13}$$

and the gain profile is

V, kn	K_{PAD}
20	1.82
40	1.74
60	1.43
80	1.51
100	1.57

Pitch Angle Pilot

This pilot provides a position control of the pitch angle by assessing the artificial horizon and operating the longitudinal cyclic stick. The relation of longitudinal cyclic to pitch angle allows the construction of a type 2 system. This provides an improved operational track and disturbance rejection. Closing the loop at $w = 3.0$ rad/sec induced a large resonant reaction in the X,Y-plane because of torque reactive disturbances. In addition, a moderate degree of very low frequency resonance was also noted in the pitch angle. The pitch angle behavior appears to be caused by the low-frequency peak-notch that was mentioned earlier. Reducing the bandwidth to $w = 1.8$ rad/sec reduced the resonant excitation and resulted in the pilot transfer function shown in

$$G_{PLT}^{THETA}(S) = \frac{K_{PT}(S + 0.8)e^{-0.2S}}{S(S + 10)} \tag{14}$$

The gain profile is

V, kn	K_{PT}
20	1.31
40	1.48
60	1.53
80	2.07
100	1.82

Roll Angle Pilot

This pilot provides a position control of the roll angle by assessing the artificial horizon and operating the lateral component of the cyclic stick. The pilot provides an integration component which allows a type 2 system configuration. Because of the extreme resonance shown in figure 15 near $w = 2.0$ rad/sec, the closed-loop pole was positioned near $w = 1.5$ rad/sec, $\delta = 0.75$. The single-variable pilot transfer function for high-speed conditions is

$$G_{PLT}^{PHI}(S)_{60,80,100} = \frac{0.68(S + 0.8)e^{-0.2S}}{S(S + 10)} \tag{15}$$

The low-speed configuration required a lesser bandwidth. The loop was closed at $w = 1.1$ rad/sec, $\delta = 0.7$. The resulting pilot transfer function is

$$G_{PLT}^{PHI}(S)_{20,40} = \frac{0.57(S + 0.8)e^{-0.2S}}{S(S + 10)} \tag{16}$$

Yaw/Directional Pilot

This pilot provides a position control of the yaw/heading angle. The integrating tendency of this configuration suggests a type 2 structure. The presence of the complex zeroes at the lower speeds caused trouble in implementing the type 2 structure because of resonant interactions with the dominant closed-loop poles. It was possible to force the poles out of this region but this caused destabilization of the higher frequency poles. To lessen the pole-zero interaction, the pilot's compensation pole was shifted to the left. The configuration is shown in figure 21. This improved the pole-zero interaction but reduced the system to a type 1. The closed-loop poles were placed near $w = 1.2$ rad/sec, $\delta = 0.55$. The resulting single-variable transfer function of the low-speed pilot mechanism is

$$G_{PLT}^{PSI}(S)_{20,40} = \frac{K_{PSL}(S + a_{PSL})e^{0.2S}}{(S + b_{PSL})(S + 10)} \tag{17}$$

The following gives the gain profiles and the compensation pole and zero placements:

V, kn	K_{PSL}	a_{PSL}	b_{PSL}
20	0.63	2.0	1.5
40	.60	1.4	.75

The high-speed configuration was not plagued by the conjugate zeroes and thus allowed a type 2 structure. The dominant closed-loop poles were placed at $w = 1.5$ rad/sec and $\delta = 0.6$ by utilizing the single-variable pilot mechanism shown in

$$G_{PLT}^{PSI}(S)_{60,80,100} = \frac{K_{PSH}(S + 0.8)e^{-0.2S}}{S(S + 10)} \tag{18}$$

The resulting gain profiles are

V, kn	K_{PSH}
60	0.43
80	.51
100	.65

RESULTS OF PILOT INSERTION

Tests and evaluations of the pilot mechanisms were performed by inserting the individual pilots into the nonlinear simulation environment. A specific flight control loop was closed by direct insertion of the associated discretized pilot mechanism within the single-variable configuration. The pilot was then subjected to various command-oriented flight maneuvers. The single-variable restriction limited the realistic operational scenarios that could be implemented.

All pilot mechanisms provided an adequate control over their specific primary variables. The secondary variables showed the anticipated wide variety of disturbed behavior. The disturbances ranged from small scale displacements and oscillations to unbounded second-order (parabolic/acceleratory) trajectories.

The following closed-loop responses were obtained with step commands from an 80-kn trimmed flight at 200 ft. The SAS and PBA were both fully engaged.

Vertical Rate Pilot

Figure 22 shows the closed-loop vertical rate response to a 10 ft/sec step command. Note the long-term lagging of the undershoot. The pilot's operation of the main rotor collective stick is shown in figure 23. Note that the control mechanism deflection is not excessive.

Figures 24 and 25 show an interesting set of responses. The intrinsic torque vector relation of this maneuver would ideally have a pronounced effect on the velocity. The ultra-low-frequency ocillations may actually emanate from the propulsion system. Figures 26 and 27 show the effects of main rotor torque disturbances on the yaw and pitch motions. The yaw angle ramp (fig. 27) is associated with the stepped increase in the main rotor torque which overpowers the trimmed counter torque supplied by the tail rotor.

Altitude Position Pilot

Figure 28 shows the closed-loop altitude position response to a 10-ft step command. A slightly more aggressive control mechanism operation is shown in figure 29. In figure 30 the yaw angle shows the effect of main rotor torque disturbances. This response can be attributed to the main rotor torque pulse

associated with this maneuver. The other vehicle reactions did not show any signs of severe disturbance.

Pitch Angle Pilot

Figure 31 shows the closed-loop response of the pitch angle to a 5° step command. Note the interesting lagged overshoot and the nonzero steady-state error in tracking. The tracking error is due to the trim tracking of the control mechanism. This can be seen in the latter phases of the longitudinal cyclic's operation (fig. 32). This is caused by the variations of the trim conditions as the velocity decreases (fig. 33). Figures 32 and 33 show the expected inverse relation between the altitude and the velocity as the main rotor's thrust vector is redirected. Figures 35 and 36 show the twisting and turning of the helicopter as it slows down. The parabolic response of the yaw angle may present problems due to its high order.

Roll Angle Pilot

Figure 37 shows the closed-loop response of the roll angle to a 10° step command. The sluggish roll angle response tends to lag the lateral cyclic stick (fig. 38). The ramped disturbance in the yaw angle (fig. 39) shows the redirection of the X,Y-component of the main rotor's thrust because of the addition of a lateral thrust component. Figure 40 shows the drop off in altitude that is expected because of the cosine reduction in the total lift vector.

Yaw Angle Pilot

Figure 41 shows the closed-loop response of the yaw angle to a 10° step command. It is interesting to note the extended overshoot behavior and the nonzero steady-state tracking error. Figure 42 shows what appears to be additional trim tracking because of the velocity stepped increase (fig. 43). Figure 44 shows the roll angle disturbance. This type of behavior is similar to tipping the wings of an airplane by operating the rudder pedals. The altitude descent (fig. 45) indicates an uncoordinated helix motion.

CONCLUDING REMARKS

The pilot mechanisms that have been developed provide adequate control of the high-performance helicopter when used in single-variable control configurations. The simple compensative response traits maintain a robust profile even though no suppression of secondary response disturbances is considered. The pilot mechanisms can therefore be used as a basis for higher level control configurations that will effectively implement the overall multivariable pilot structure as a group of these mechanisms.

The companion report (ref. 4) to this one gives one way of doing this. It is recommended that additional research be conducted to use various forms of adaptive and learning processes to further improve the overall effectiveness of the pilot mechanisms.

APPENDIX - DEFINITION OF VARIABLES

The variables are referenced to a local nonrotating frame which originates at the center of gravity of the helicopter with axes parallel to, but offset from, a flat Earth inertial frame. X_L, Y_L, and Z_L represent these axes; x_b, y_b, and z_b represent axes fixed in the helicopter's body with origin at the center of gravity.

Longitudinal Variables

X,Z-plane:

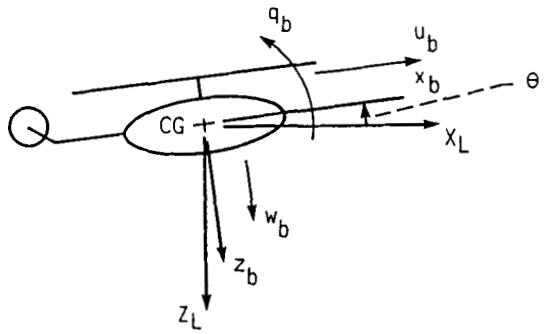

$$\theta \equiv \int q_b \cos \phi - r_b \sin \phi \, dt$$

q_b perturbation pitch rate in body axis

r_n Euler roll angle

u_n velocity perturbation along X-body

w_n velocity perturbation along Z-body

X_L X-component of local frame

x_n X-body component

Z_L Z-component of local frame

z_b Z-body component

θ Euler pitch angle

ϕ Euler roll angle

Lateral Variables

X,Y-plane:

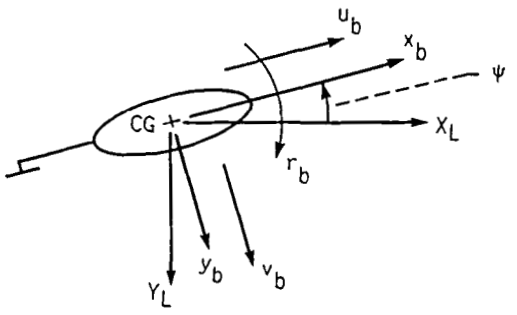

$$\psi \equiv \int \frac{r_b \cos \phi + q_b \sin \phi}{\cos \theta}$$

r_b perturbation yaw rate in body axis

v_b velocity perturbation along Y-body axis

Y_L Y-component of local frame

y_b Y-body component

ψ Euler yaw angle

Y,Z-plane:

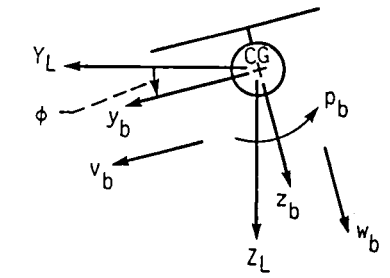

$$\phi \equiv \int p_b + \dot{\psi} \sin \Theta \, dt$$

p_b perturbation roll rate in body axis

ϕ Euler roll angle

Airstream Variables

Vehicle angle of attack:

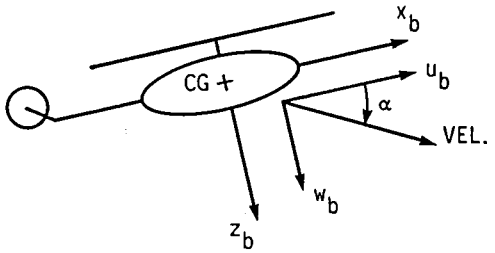

$$\alpha = \text{TAN}^{-1}\left[\frac{w_b}{u_b}\right]$$

Vehicle sideslip angle:

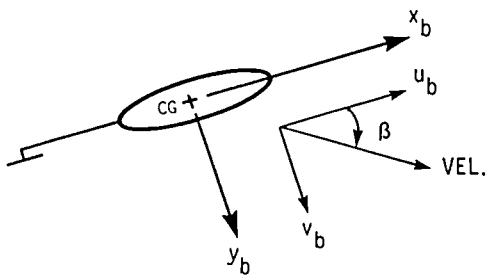

$$\beta = \text{TAN}^{-1}\left[\frac{v_b}{|u_b + w_b|}\right]$$

REFERENCES

1. Howlett, J.J.: UH-60A Black Hawk Engineering Simulation Program, Vol. 1, Mathematical Model. (ISER-70452, Sikorsky Aircraft; NASA Contract NAS2-10626), NASA CR-166309, 1981.

2. McRuer, D.T.; and Krendal, E.S.: Dynamic Response of Human Operators. Wright Air Development Center, WADC TR-56-524, Oct. 1957. (Avail. NTIS, AD-110693.)

3. Mayhew, B.H.: Multivariable Digital Control Laws For The UH-60A Black Hawk Helicopter. M.S. Thesis, Air Force Institute of Technology, 1984. (Avail. NTIS, AD-A141046.)

4. Zipf, M.E., et al.: Computer Simulation of a Single Pilot Flying a Modern High-Performance Helicopter. NASA TM-100182, 1988.

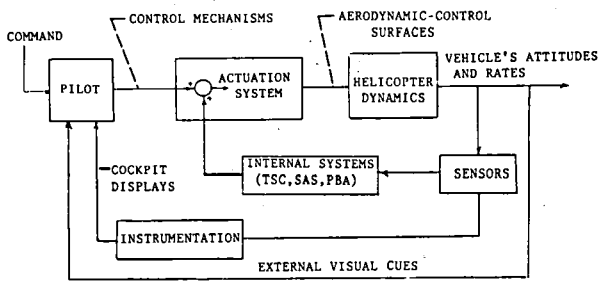

FIGURE 1. - BLOCK DIAGRAM OF PILOT IN LOOP CONTROL STRUCTURE.

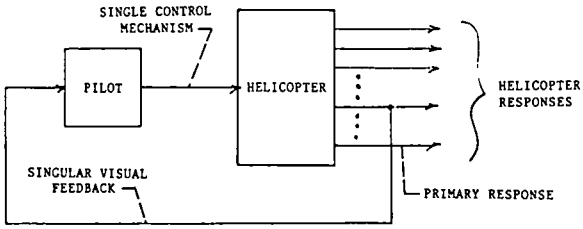

FIGURE 2. - SINGLE-VARIABLE CONTROL STRUCTURE BASED ON DOMINANT VEHICLE RESPONSES.

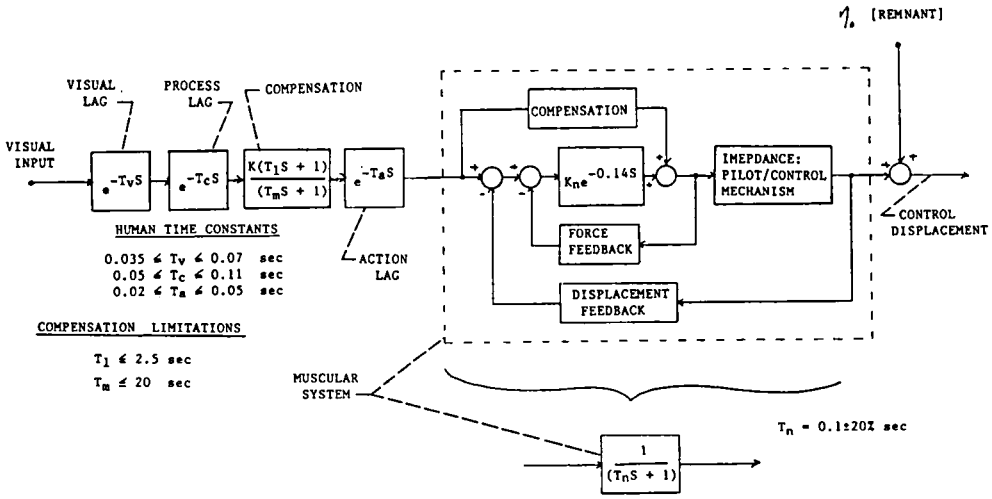

FIGURE 3. - BLOCK DIAGRAM OF McRUER-KRENDAL HUMAN RESPONSE MECHANISM.

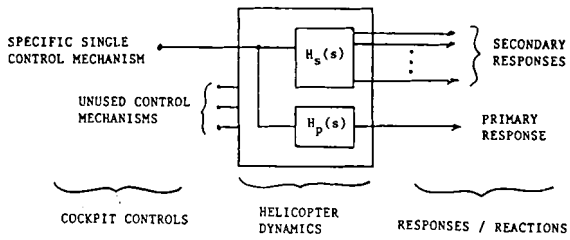

FIGURE 4. - DOMINANT RESPONSE MODEL FOR SINGLE-VARIABLE CONTROL MECHANISMS.

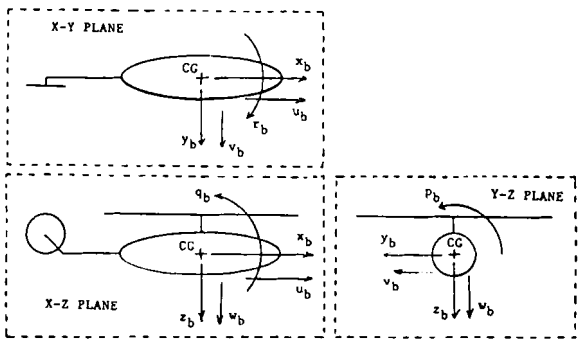

FIGURE 5. - HELICOPTER DESCRIPTION WITHIN ORTHOGONAL CONTROL PLANES.

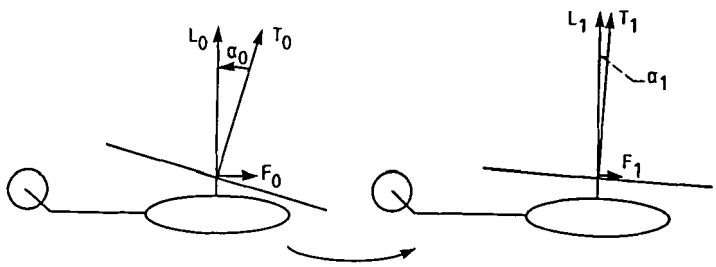

FIGURE 6. - SIMPLIFIED ILLUSTRATION OF EFFECTS OF BACKWARD DEFLECTION OF LONGITUDINAL CYCLIC STICK. ANGLE OF ATTACK, α_i.

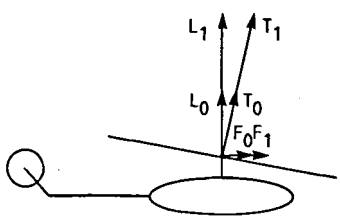

FIGURE 7. - SIMPLIFIED ILLUSTRATION OF EFFECTS OF UPWARD DEFLECTION OF MAIN ROTOR COLLECTIVE STICK.

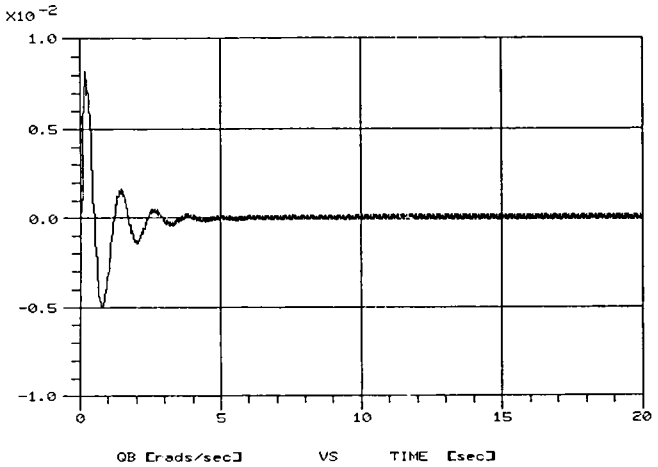

FIGURE 8. - TIME RESPONSE OF PITCH RATE DUE TO IMPULSE ON LONGITUDINAL CYCLIC STICK AT 60 KN.

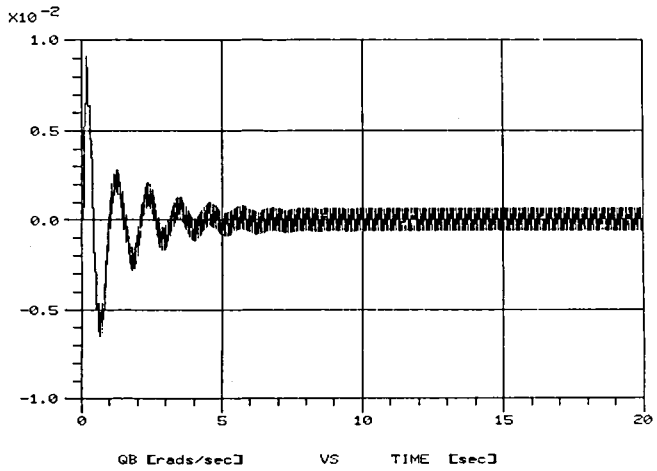

FIGURE 9. - TIME RESPONSE OF PITCH RATE DUE TO IMPULSE ON LONGITUDINAL CYCLIC STICK AT 100 KN.

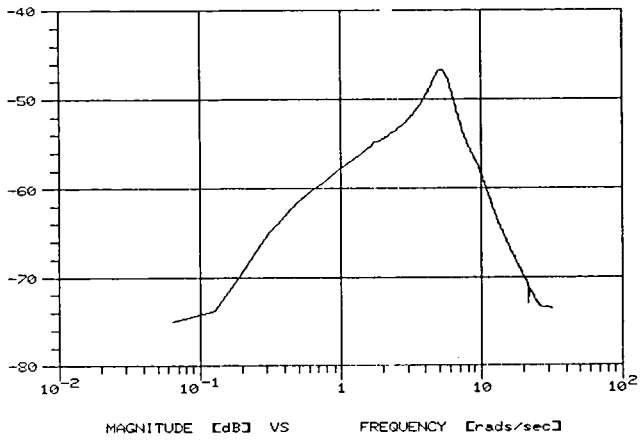

FIGURE 10. - FAST FOURIER TRANSFORM (FFT) OF IMPULSE RESPONSE OF PITCH RATE AT 60 KN.

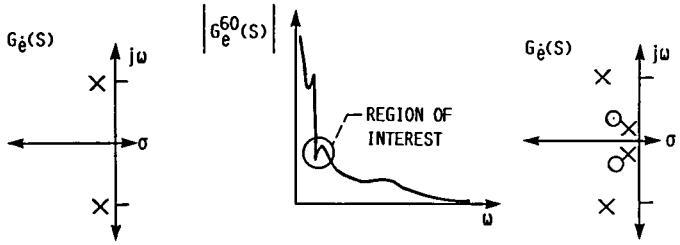

(a) LOW-ORDER LAPLACE PLANE REPRESENTATION OF PITCH RATE.

(b) FREQUENCY RESPONSE OF PITCH ANGLE.

(c) HIGHER ORDER LAPLACE PLANE REPRESENTATION OF PITCH RATE.

FIGURE 11. - VEHICLE PITCH DESCRIPTIONS BASED ON LONGITUDINAL CYCLIC STICK DEFLECTIONS.

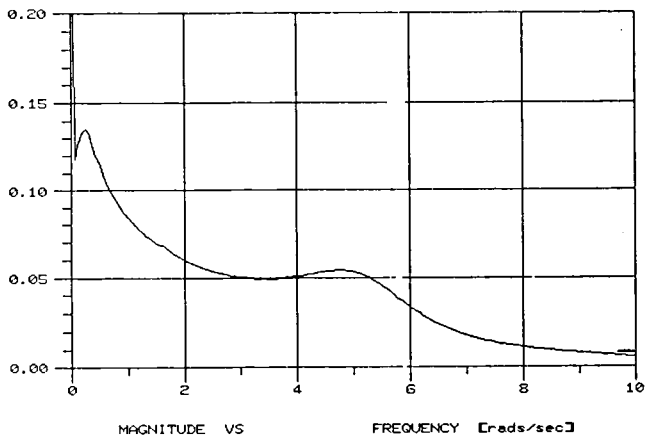

FIGURE 12. - FAST FOURIER TRANSFORM (FFT) OF IMPULSE RESPONSE OF PITCH ANGLE AT 60 KN.

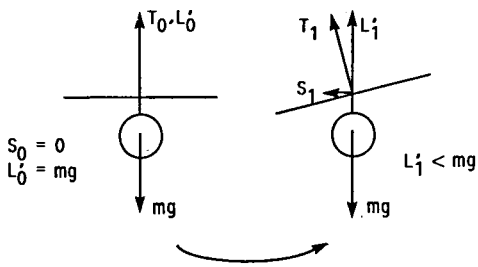

FIGURE 13. - SIMPLIFIED ILLUSTRATION OF EFFECTS OF RIGHTWARD DEFLECTION OF LONGITUDINAL CYCLIC STICK.

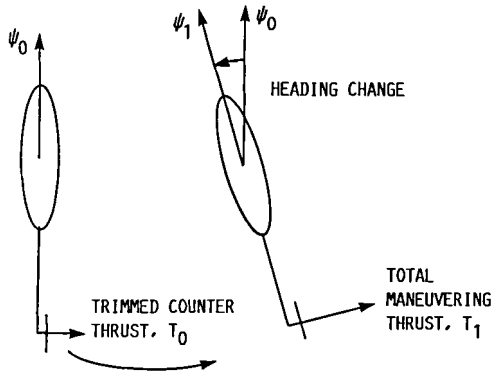

FIGURE 14. - SIMPLIFIED ILLUSTRATION OF EFFECTS OF CLOCKWISE ROTATION OF TAIL ROTOR COLLECTIVE PEDALS.

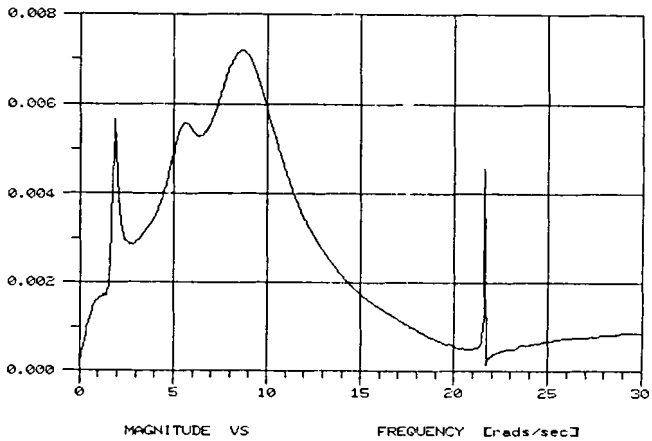

FIGURE 15. - FAST FOURIER TRANSFORM (FFT) OF IMPULSE RESPONSE OF ROLL RATE AT 80 KN.

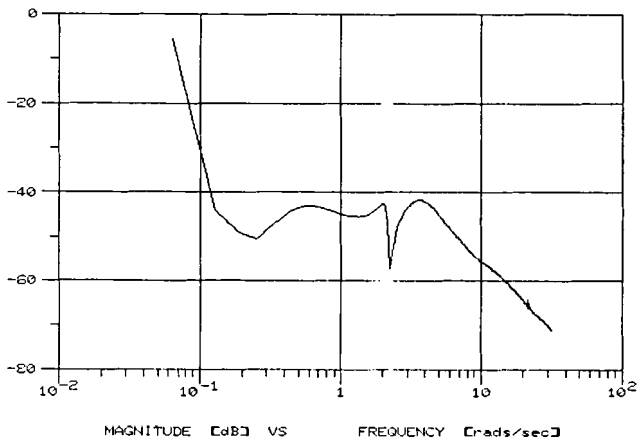

FIGURE 16. - FAST FOURIER TRANSFORM (FFT) OF IMPULSE RESPONSE OF YAW RATE AT 20 KN.

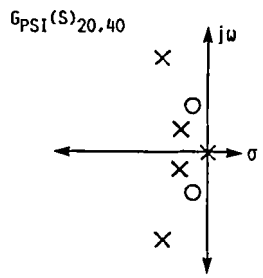

FIGURE 17. - LOW-ORDER LAPLACE PLANE REPRESENTATION OF YAW ANGLE FROM TAIL ROTOR COLLECTIVE PEDAL DEFLECTION.

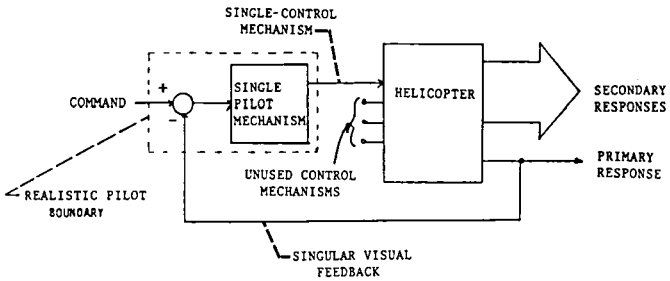

FIGURE 18. - BLOCK DIAGRAM OF SINGLE-VARIABLE PILOT MECHANISM WITHIN DOMINANT RESPONSE CONTROL LOOP.

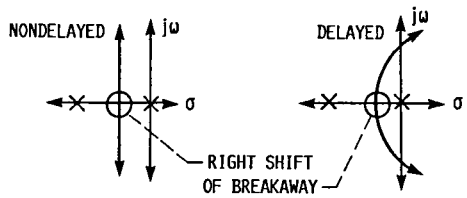

FIGURE 19. - COMPARATIVE ILLUSTRATION OF DISTORSION OF DELAYED ROOT LOCUS VERSUS A NON-DELAYED ROOT LOCUS.

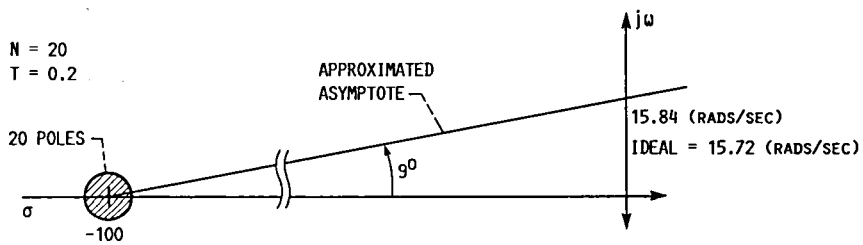

FIGURE 20. - ILLUSTRATION OF PRIMARY ASYMPTOTES OF PURE DELAY APPROXIMATION.

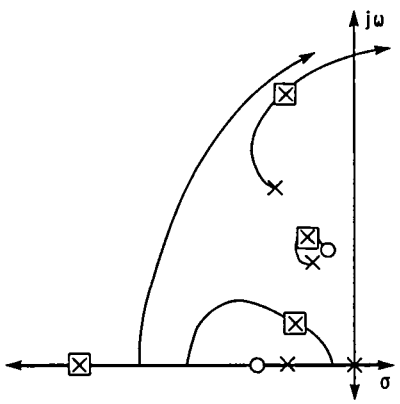

FIGURE 21. - ROOT LOCUS OF CLOSED-LOOP POLES OF YAW ANGLE CONTROL LOOP AT 20 KN.

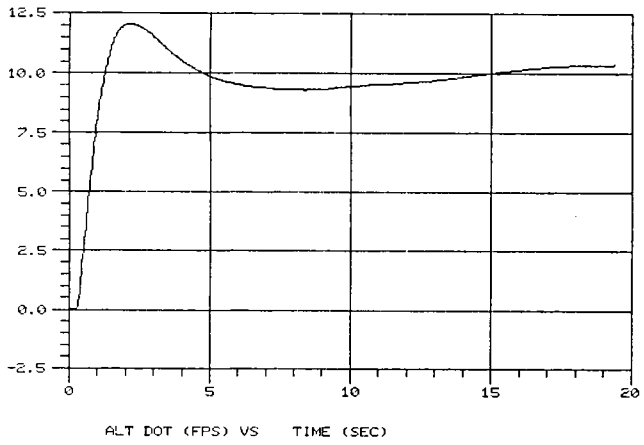

FIGURE 22. - CLOSED-LOOP STEP RESPONSE OF SINGLE-VARIABLE VERTICAL RATE CONTROL AT 80 KN.

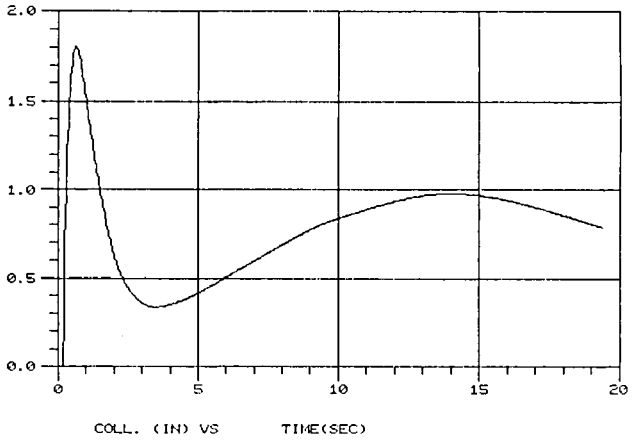

FIGURE 23. - MAIN ROTOR COLLECTIVE STICK DEFLECTION BY HUMAN RESPONSE MECHANISM TO ACHIEVE STEP MANEUVER IN FIGURE 22.

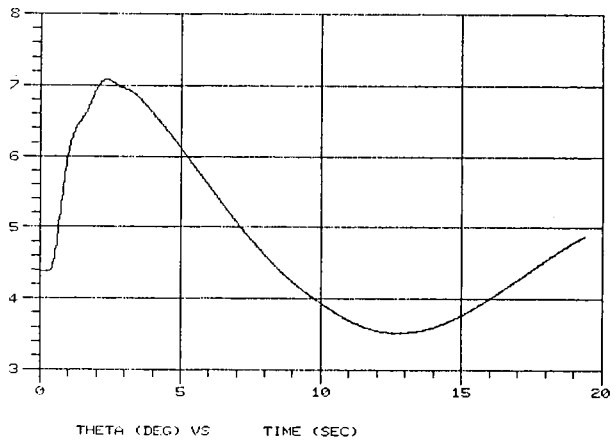

FIGURE 24. - PITCH ANGLE REACTION DUE TO STEP IN VERTICAL RATE.

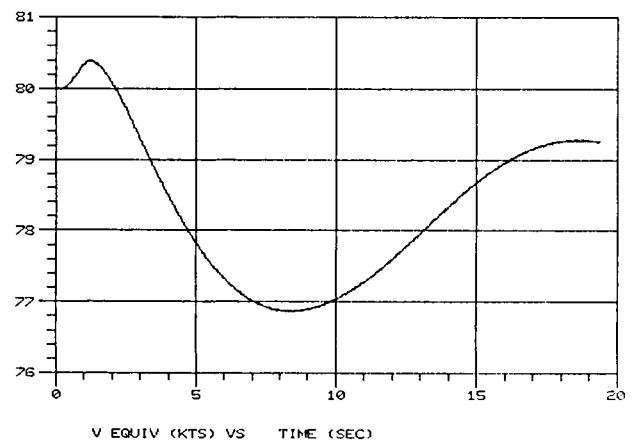

FIGURE 25. - VELOCITY REACTION DUE TO STEP IN VERTICAL RATE.

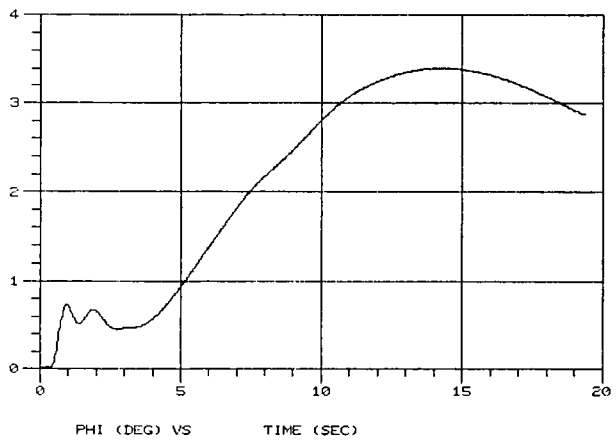

FIGURE 26. - ROLL ANGLE REACTION DUE TO STEP IN VERTICAL RATE.

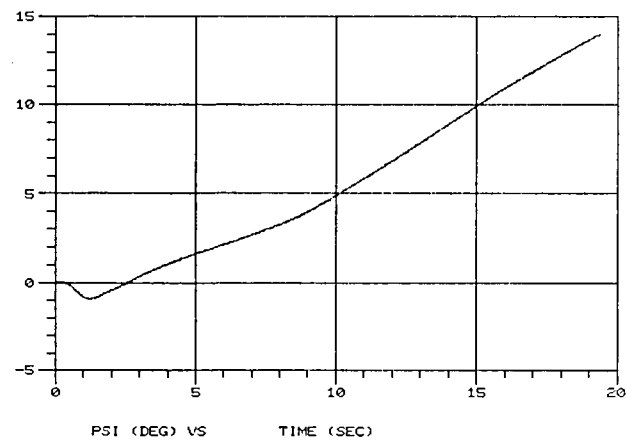

FIGURE 27. - YAW ANGLE REACTION DUE TO STEP IN VERTICAL RATE.

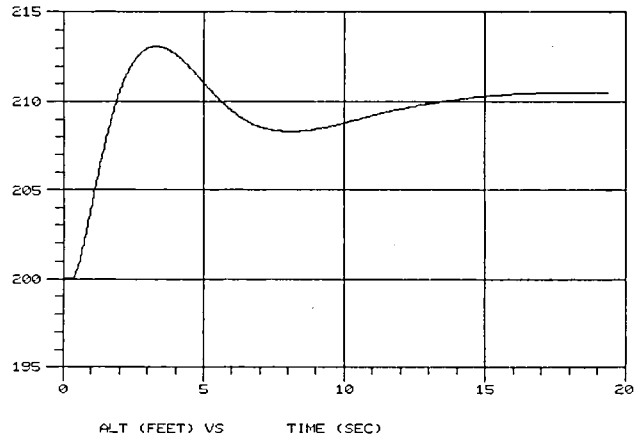

FIGURE 28. - CLOSED-LOOP STEP RESPONSE OF SINGLE-VARIABLE ALTITUDE CONTROL AT 80 KN.

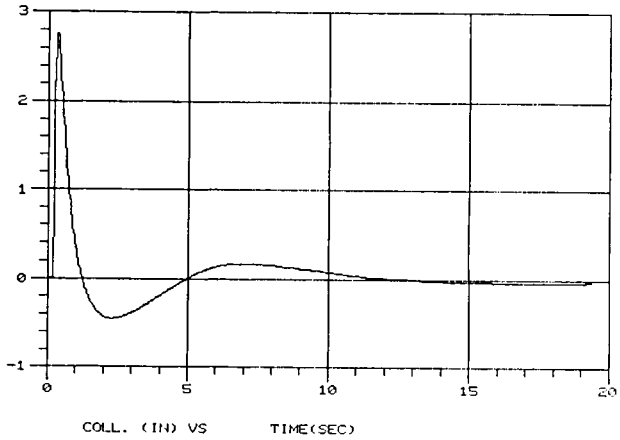

FIGURE 29. - MAIN ROTOR COLLECTIVE STICK DEFLECTION BY HUMAN RESPONSE MECHANISM TO ACHIEVE STEP MANEUVER IN FIGURE 28.

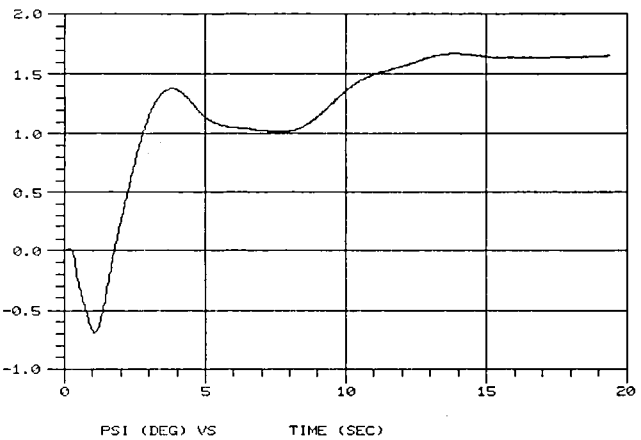

FIGURE 30. - YAW ANGLE REACTION DUE TO STEP IN ALTITUDE.

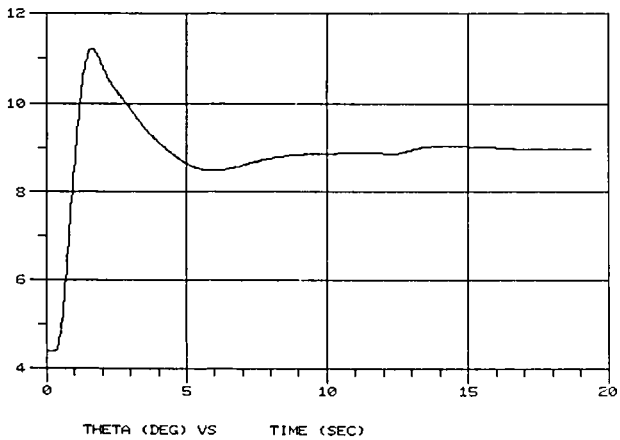

FIGURE 31. - CLOSED-LOOP STEP RESPONSE OF SINGLE-VARIABLE PITCH ANGLE CONTROL AT 80 KN.

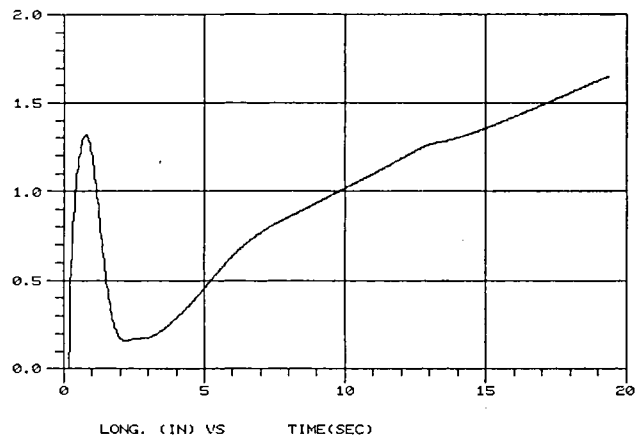

FIGURE 32. - LONGITUDINAL CYCLIC STICK DEFLECTION BY HUMAN RESPONSE MECHANISM TO ACHIEVE STEP MANEUVER IN FIGURE 31.

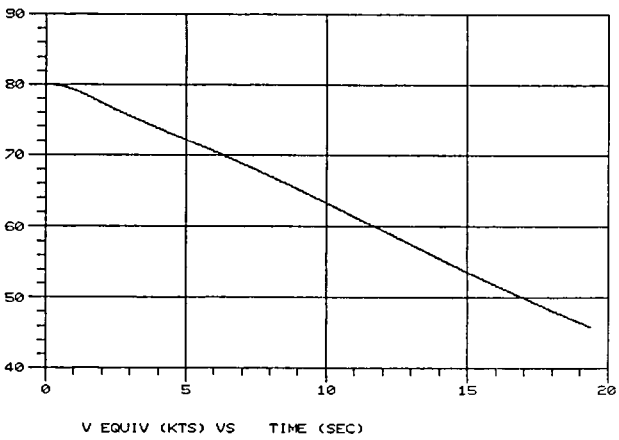

FIGURE 33. - VELOCITY REACTION DUE TO STEP IN PITCH ANGLE.

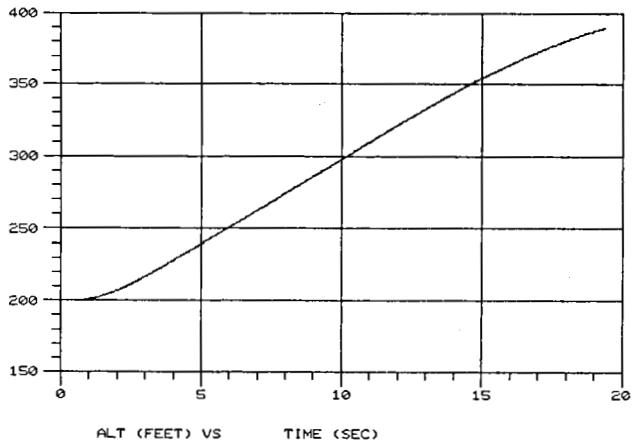

FIGURE 34. - ALTITUDE REACTION DUE TO STEP IN PITCH ANGLE.

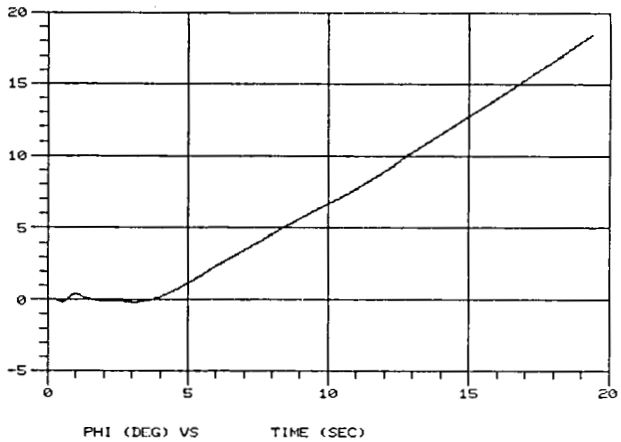

FIGURE 35. - ROLL ANGLE REACTION DUE TO STEP IN PITCH ANGLE.

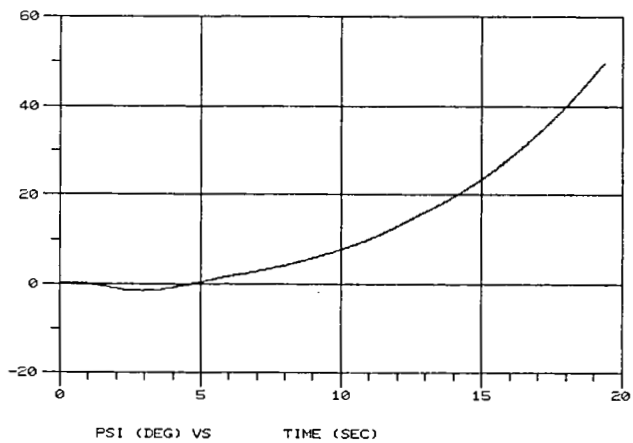

FIGURE 36. - YAW ANGLE REACTION DUE TO STEP IN PITCH ANGLE.

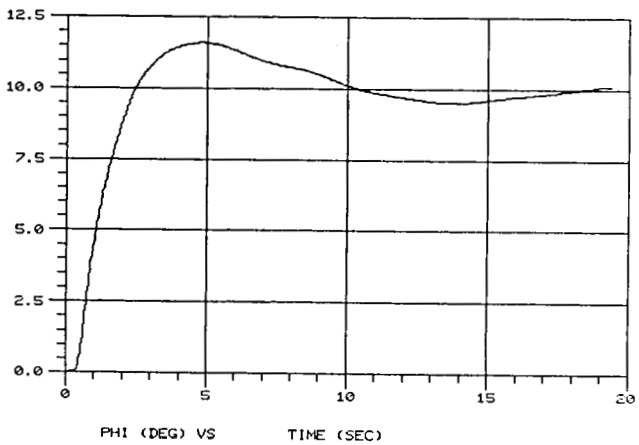

FIGURE 37. - CLOSED-LOOP STEP RESPONSE OF SINGLE-VARIABLE ROLL ANGLE CONTROL AT 80 KN.

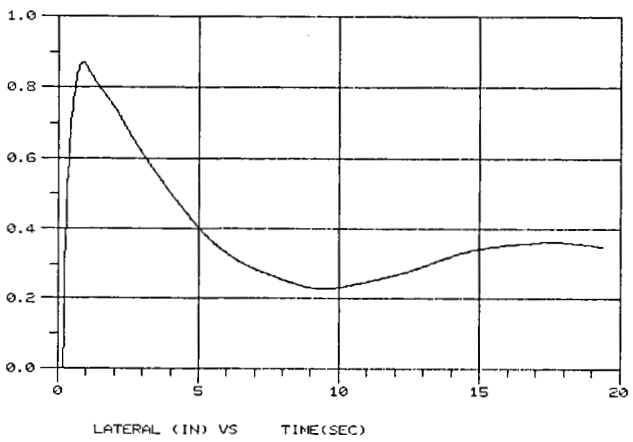

FIGURE 38. - LATERAL CYCLIC STICK DEFLECTION BY HUMAN RESPONSE MECHANISM TO ACHIEVE STEP MANEUVER IN FIGURE 37.

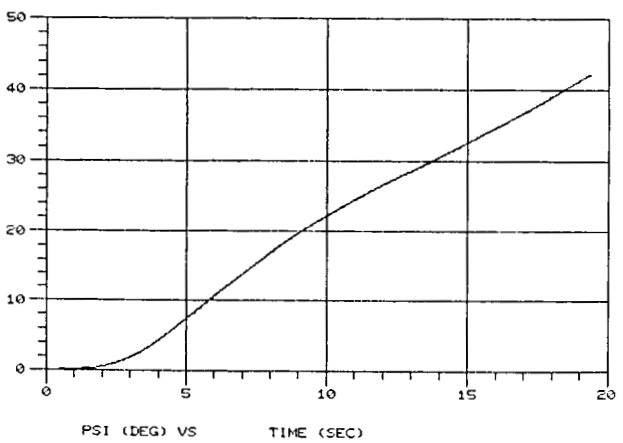

FIGURE 39. - YAW ANGLE REACTION DUE TO STEP IN ROLL ANGLE.

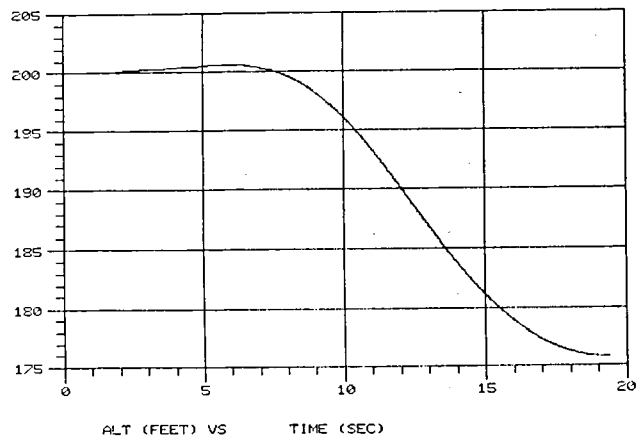

FIGURE 40. - ALTITUDE REACTION DUE TO STEP IN ROLL ANGLE.

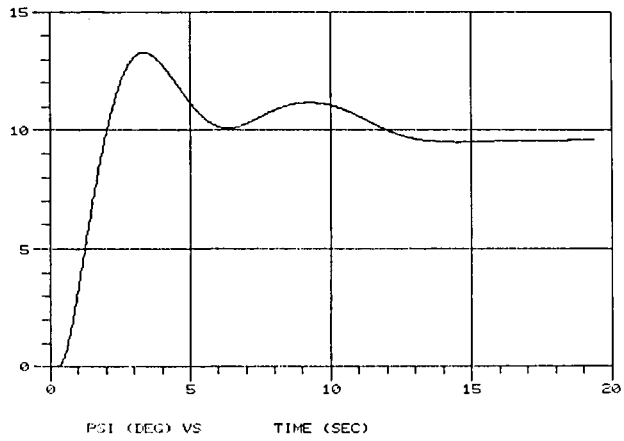

FIGURE 41. - CLOSED-LOOP STEP RESPONSE OF SINGLE-VARIABLE YAW ANGLE CONTROL AT 80 KN.

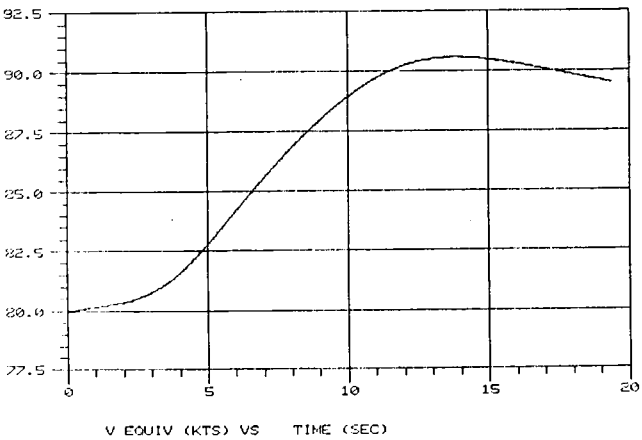

FIGURE 42. - TAIL ROTOR COLLECTIVE PEDAL DEFLECTION BY HUMAN RESPONSE MECHANISM TO ACHIEVE STEP MANEUVER IN FIGURE 41.

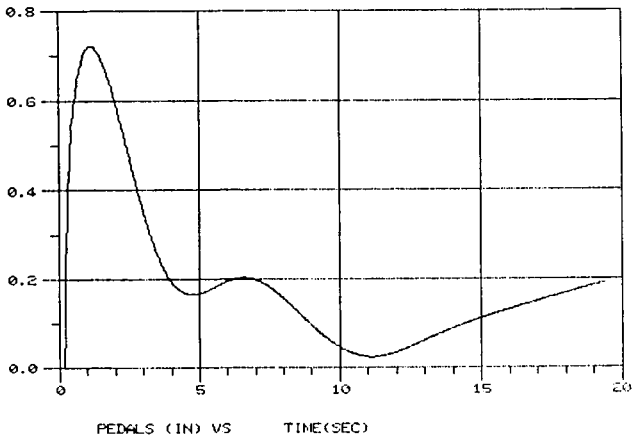

FIGURE 43. - VELOCITY REACTION DUE TO STEP IN YAW ANGLE.

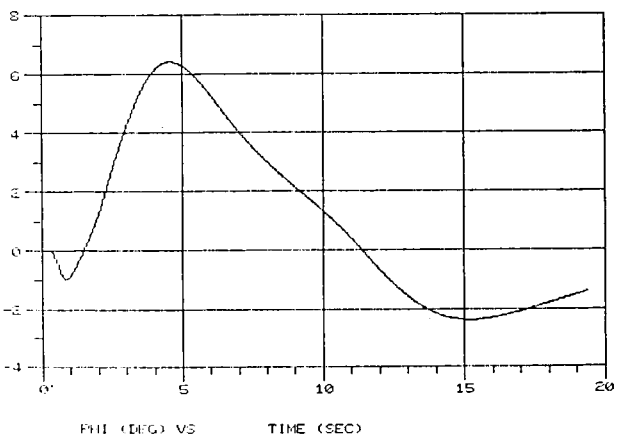

FIGURE 44. - ROLL ANGLE REACTION DUE TO STEP IN YAW ANGLE.

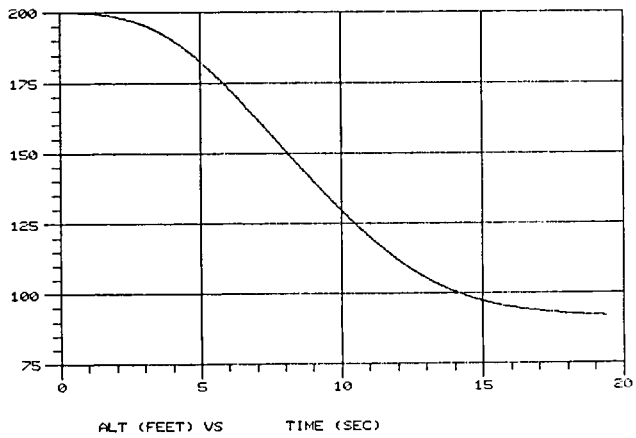

FIGURE 45. - ALTITUDE REACTION DUE TO STEP IN YAW ANGLE.

NASA
National Aeronautics and Space Administration

Report Documentation Page

1. Report No.	2. Government Accession No.	3. Recipient's Catalog No.
NASA TM-100183		

4. Title and Subtitle	5. Report Date
Computer Simulation of Multiple Pilots Flying a Modern High-Performance Helicopter	July 1988
	6. Performing Organization Code

7. Author(s)	8. Performing Organization Report No.
Mark E. Zipf, William G. Vogt, Marlin H. Mickle, Ronald G. Hoelzeman, Fei Kai, and James R. Mihaloew	E-3760
	10. Work Unit No. 505-90-01

9. Performing Organization Name and Address	11. Contract or Grant No.
National Aeronautics and Space Administration Lewis Research Center Cleveland, Ohio 44135-3191	
	13. Type of Report and Period Covered
12. Sponsoring Agency Name and Address	Technical Memorandum
National Aeronautics and Space Administration Washington, D.C. 20546-0001	14. Sponsoring Agency Code

15. Supplementary Notes

Mark E. Zipf, William G. Vogt, Marlin H. Mickle, Ronald G. Hoelzeman, and Fei Kai, Department of Electrical Engineering, University of Pittsburgh, Pittsburgh, Pennsylvania (work funded by NASA Grant NAG3-729); James R. Mihaloew, NASA Lewis Research Center.

16. Abstract

A computer simulation of a human response pilot mechanism within the flight control loop of a high-performance modern helicopter is presented. A human response mechanism, implemented by a low order, linear transfer function, is used in a decoupled single variable configuration that exploits the dominant vehicle characteristics by associating cockpit controls and instrumentation with specific vehicle dynamics. Low order helicopter models obtained from evaluations of the time and frequency domain responses of a nonlinear simulation model, provided by NASA Lewis Research Center, are presented and considered in the discussion of the pilot development. Pilot responses and reactions to test maneuvers are presented and discussed. Higher level implementation, using the pilot mechanisms, are discussed and considered for their use in a comprehensive control structure.

17. Key Words (Suggested by Author(s))	18. Distribution Statement
Simulation Paper pilot	Unclassified - Unlimited Subject Category 08

19. Security Classif. (of this report)	20. Security Classif. (of this page)	21. No of pages	22. Price*
Unclassified	Unclassified	32	A02

*For sale by the National Technical Information Service, Springfield, Virginia 22161